coatings

MDPI

Article

Different Approaches to Low-Wettable Materials for Freezing Environments: Design, Performance and Durability

Giulio Boveri, Alessandro Corozzi *, Federico Veronesi and Mariarosa Raimondo

Institute of Science and Technology for Ceramics, National Research Council (ISTEC CNR), Via Granarolo, 64, 48018 Faenza, Italy; giulioboveri01@gmail.com (G.B.); federico.veronesi@istec.cnr.it (F.V.); mariarosa.raimondo@istec.cnr.it (M.R.)

* Correspondence: alessandro.corozzi@istec.cnr.it; Tel.: +39-0546-699-776

Abstract: Ice nucleation and accretion leads to multiple problems such as freezing of the streets which can cause traffic collisions or people injuries, and collapse of high voltage power lines leading to black-out and icing of aircraft components, causing major aeronautic accidents. The most widespread strategies for the removal of accumulated ice layers result in most cases being expensive, time-consuming and hazardous for the environment. In this work we present the design of hydrophobic hybrid inorganic-organic coatings via Lotus leaf-like and slippery liquid infused porous surfaces (SLIPS) approaches with reduced, lasting wetting performance in cold environments. Static and dynamic wetting behavior was evaluated at room and sub-zero temperatures. The main target was the selection of the most suitable design approaches and formulations of coatings to be applied on metals or alloys when the contact time between the droplet and the material surface has to be minimized. In the temperature range from −10 to 0 °C, we report evidence of a stable hydrophobicity and a low water contact angle hysteresis (below 15°) of all the SLIPS developed. The surfaces' ability to keep their wetting performance unchanged during the freeze/and frost/thaw durability cycles stood out as a key issue for further development at larger scale.

Keywords: anti-icing; bio-inspired; drop-mobility; contact time; nanostructured surfaces; hybrid coatings; sol gel; hydrophobicity

check for updates

Citation: Boveri, G.; Corozzi, A.; Veronesi, F.; Raimondo, M. Different Approaches to Low-Wettable Materials for Freezing Environments: Design, Performance and Durability. *Coatings* **2021**, *11*, 77. https://doi.org/10.3390/coatings11010077

Received: 23 December 2020
Accepted: 5 January 2021
Published: 11 January 2021

Publisher's Note: MDPI stays neutral with regard to jurisdictional claims in published maps and institutional affiliations.

Copyright: © 2021 by the authors. Licensee MDPI, Basel, Switzerland. This article is an open access article distributed under the terms and conditions of the Creative Commons Attribution (CC BY) license (https://creativecommons.org/licenses/by/4.0/).

1. Introduction

The interaction between water in many different forms—either liquid or solid like dry or wet snow, ice, frost, rime or combinations thereof—and a solid surface at a subzero temperature is a complex matter to investigate, depending on many material-related parameters, e.g., surface chemical composition and texturing, and environmental conditions such as temperature, humidity, wind velocity, etc.

The formation and the following accretion of different forms of solid water on structural installations, facilities and infrastructures, aeronautic components, telecommunication systems and so on represents a huge problem in cold regions or under specific operational contexts. For example, nucleation and growth of ice and/or snow accumulation on roads often leads to car accidents, while the accretion of ice on aircraft wings, in particular during the takeoff and landing operations, has to be avoided for passenger security. To date, in order to mitigate such phenomena, the most widespread and effective strategies for the removal of accumulated ice layers are based on the Joule effect, mechanical removal, electro-impulse methods or application of de-icing fluids [1–4]. However, these traditional procedures are in most cases expensive, time-consuming and hazardous for the environment.

In this framework, many authors refer to the generally called anti-icing materials and technologies as a solution to prevent or delay nucleation, adhesion and accumulation of dry/wet snow, frost, rime, ice, or their combination, according to the specific environmental conditions.

Superhydrophobic (SH) surfaces, due to their advanced water repellency, have been actively investigated as candidate anti-icing materials [5–11]. These materials are expected to avoid the accretion of solid water thanks to the high mobility that liquid water drops show on their surface, coupled with a lower heat exchange rate and a decrease of the contact area [12,13], thus avoiding solidification of supercooled liquid water droplets that form in tropospheric clouds, an extremely dangerous phenomenon for aircraft [14]. Most of the technical solutions to SH materials are achieved by introducing surface modifications at two different levels: (i) a physical modification to get hierarchical micro-nano structural features entrapping air; and (ii) a chemical modification to lower the surface energy. In this way, a Cassie–Baxter wetting state is obtained, characterized by very limited interactions between the solid surface and the water drops, resulting in a static water contact angle (WCA) higher than 150° and contact angle hysteresis (CAH) lower than 10°. Hierarchical morphology obtained in the Cassie-Baxter wetting state leads to the trapping of several pockets of air between the nano-features, which should act as a thermal insulator, as described in different scientific papers in the last years [15,16]. When practical applications for SH materials are taken into account, the main hindrance is generally represented by their durability, since under abrasion, erosion or other severe conditions the peculiar structural features might be easily destroyed [10,17,18], allowing water drops to penetrate into the structure annihilating the Cassie-Baxter wetting state and nullifying the SH behavior. Moreover, in environments with high relative humidity, condensation of tiny water drops can occur between the surface features of SH surfaces, again leading to the disruption of the Cassie–Baxter wetting state [19].

In order to overcome the issues connected to the structural weakness of Lotus leaf-like surfaces, in the last years scientists considered new design approaches and, among them, the one leading to the slippery liquid infused porous surfaces (SLIPS) [20]. These innovative surfaces are based on the infusion of a liquid, e.g., a lubricant, that wicks into a porous material to make it repellent to a wide range of liquids in conditions where SH usually fail, like humid and high-pressure environments. Several types of SLIPS have been specifically designed for applications in icing conditions. Different research groups [21,22] developed liquid-infused surfaces that effectively suppressed ice/frost accretion by removing condensed moisture, coupled with good resistance to icing/deicing cycles. More recently Wei et al. [23] demonstrated a decrease of 3 orders of magnitude of ice adhesion on slippery surfaces if compared with Lotus leaf-inspired ones. Even though using a SLIPS approach might sensibly delay and reduce the formation and/or the adhesion of ice, liquid-infused surfaces exhibit a new failure mode: the infused liquid film may drain due to an external shear flow, causing the surface to lose its advantageous properties [24,25]. Moreover, the mechanisms underlying the anti-icing behavior of these liquid-repellent surfaces are still under debate. Several recent papers concern the dependence of ice nucleation and accretion on the contact time between supercooled water droplets and low-wettable surfaces. Mishchenko et al. [26] specifically highlighted the relationship between the dynamic repellency to liquids and the attitude to ice nucleation and accretion of different coated surfaces. On surfaces with CAH as low as 15°, a full retraction of the supercooled drops is expected before ice nucleation occurs. Khedir et al. [27] found a complete drop rebound at temperatures as low as −10 °C on SH Teflon-coated surfaces, suggesting their potential anti-icing properties in aeronautical applications. Poulikakos' group [28] studied the impact of supercooled droplets on SH surfaces, highlighting the role of water viscosity on the penetration in the structural features of coatings occurring at subzero temperatures. The key parameter in this case is the CAH of the developed surfaces; high dynamic behavior allows the decrease of the contact time of the droplets on the materials, avoiding the nucleation and accretion of ice [29].

In our work, we designed hybrid organic-inorganic layers able to generate hierarchically organized coatings with advanced water repellency. In terms of the design approach, we fabricated SH surfaces mimicking the Lotus Leaf (labeled as LF) and SLIPS. In both cases, the fabricated hybrid coatings comprise an inorganic, porous layer based on ceramic

(Al_2O_3, SiO_2) nanoparticles obtained via sol-gel, while the organic layer consists of fluoroalkylsilane molecules. For SLIPS, either a fluorinated oil or a fluorine-free silicone oil was infused in the porous hybrid coatings. Then, static and dynamic wetting properties of LF and SLIPS materials were evaluated via goniometric measurements at room and sub-zero temperatures, with the aim of selecting the most suitable chemical and textural features to maximize water drop mobility in freezing conditions. The target is to select coating candidates for those applications (e.g., aeronautic icing mitigation) in which the time of contact between the droplet and the material surface has to be minimized. In perspective of an application in real conditions, the ability of coated materials to keep unchanged their wetting performance over the time is considered as a key issue. Therefore, durability of LF and SLIPS samples was assessed by monitoring the change in CAH after freeze/and frost/thaw cycles, in presence or absence of water, respectively.

2. Materials and Methods

2.1. Preparation of Alumina Sol

Alcoholic alumina sol was prepared as described in a previous work [30]. Aluminum-tri-sec-butoxide (97%, Sigma-Aldrich, Darmstadt, Germany) was stirred in isopropyl alcohol (99%, Sigma-Aldrich) for 1 h at room temperature. Then, ethyl acetoacetate (99%, Sigma-Aldrich) as the chelating agent was added and the solution was stirred for 3 h. Finally, water was gradually added to the solution to promote the hydrolysis of the alkoxide, keeping the sol under stirring for 24 h at room temperature. The particle size distribution of the sol was evaluated by dynamic light scattering (DLS) (Zetasizer Nano S, Malvern Instruments, Malvern, UK). The sol showed a multimodal particle size distribution (Figure 1). The peak with the highest scattering intensity is centered at 2.2 nm with smaller amounts of aggregated particles.

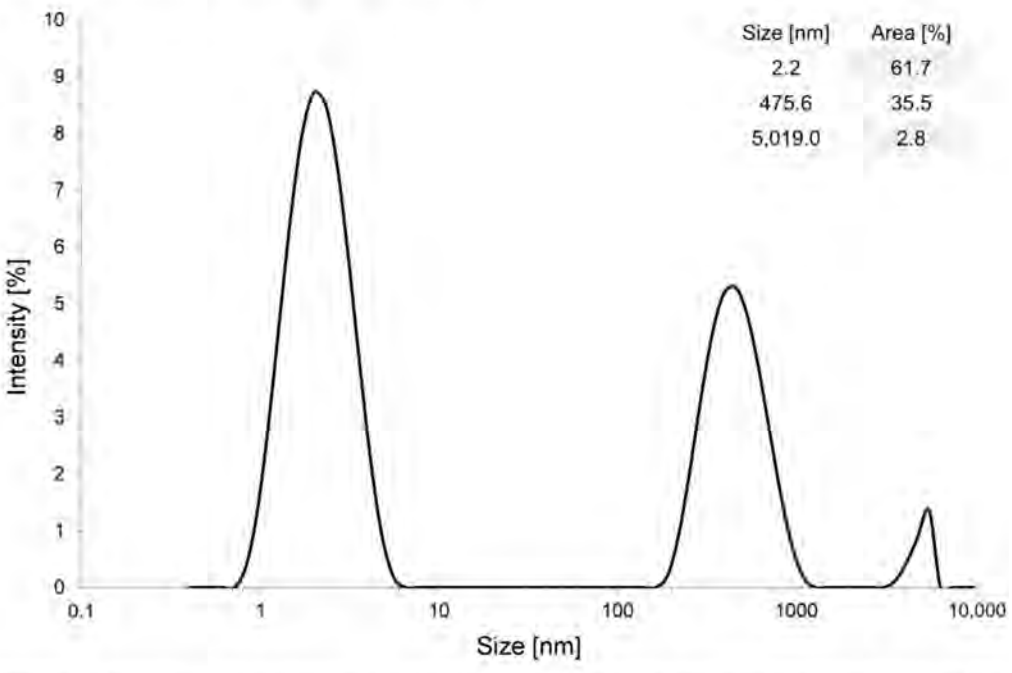

Figure 1. Dynamic light scattering (DLS) spectrum showing the particle size distribution in the alumina sol. Mean size values for each peak and corresponding scattering intensity percentages are reported in the inset table.

2.2. Preparation of Silica Nano-Suspension

The suspension of fluorine-bearing silica nanoparticles was prepared as follows: ammonium hydroxide NH_4OH (30%, Sigma-Aldrich) was added to ethanol (99%, Sigma-Aldrich) and stirred to complete dissolution. Then, tetraethylorthosilicate (TEOS 98%,

Sigma-Aldrich) was introduced in the solution, setting the temperature at 60 °C. Once the temperature was reached, 1H,1H,2H,2H-perfluoroctyltriethoxysilane (PFOTS 98%, Sigma Aldrich) was added in the solution, enhancing the hydrophobic behavior of the silica nanoparticles. The particle size distribution of the suspension was evaluated by DLS. The spectrum of the nanoparticle suspension exhibits a monodisperse size distribution (PdI = 0.1) with a clear peak positioned at 481 nm (Figure 2).

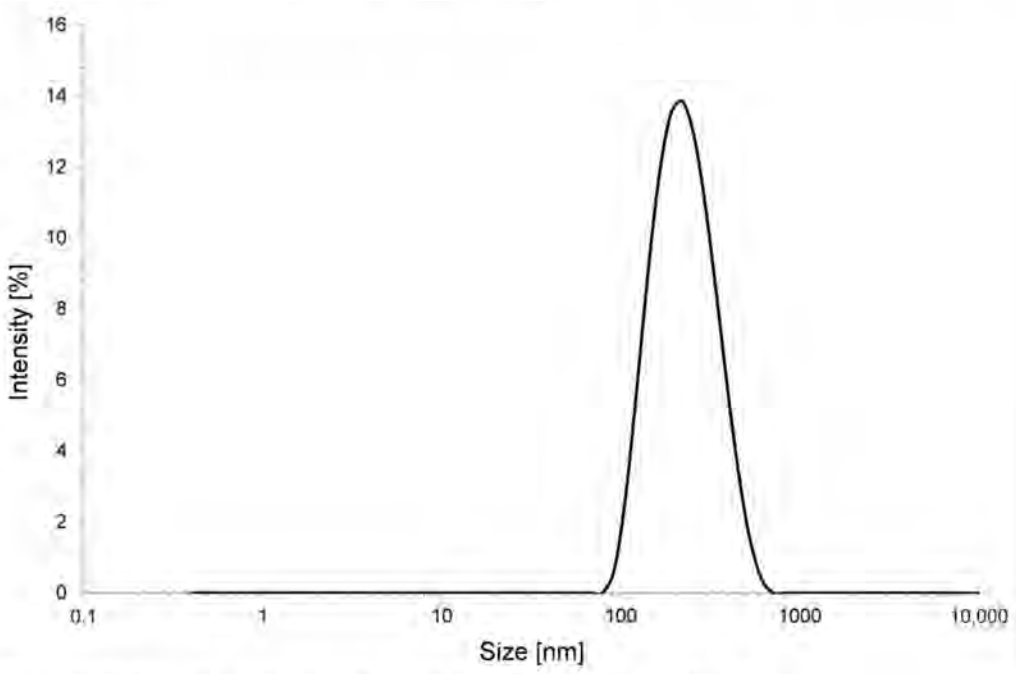

Figure 2. DLS spectrum showing the particle size distribution in the silica.

2.3. Production of LF and SLIPS Samples by Deposition of Hybrid Coatings

Aluminum alloy foils with dimensions of 2 × 2 cm^2 and a surface roughness Ra of about 0.5 µm were used as substrate. After cleaning with soapy water and ethanol to remove impurities, they were processed as detailed in the next sections. Dip coating under controlled conditions was chosen as the deposition technique due to the low cost of equipment, its flexibility and operational simplicity for the processing of materials with different sizes and morphologies. Samples details are summarized in Table 1.

Table 1. Summary of the tested coating compositions.

Sample	Inorganic Layer	Organic Layer	Lubricant
LF	Alumina	FAS	/
Al_2O_3Kr100	Alumina	FAS	Krytox™ GPL 100
Al_2O_3Kr103	Alumina	FAS	Krytox™ GPL 103
Al_2O_3Kr105	Alumina	FAS	Krytox™ GPL 105
SiO_2F SO10	Fluorinated Silica	/	Silicone oil 10cSt
SiO_2FKr100	Fluorinated Silica	/	Krytox™ GPL 100
SiO_2FKr103	Fluorinated Silica	/	Krytox™ GPL 103
SiO_2FKr105	Fluorinated Silica	/	Krytox™ GPL 105

LF sample substrates were dip-coated in the alumina sol with a dipping-withdrawal speed of 2 mm/s and a soaking time of 5 s. After drying at room temperature, they were annealed at 400 °C for 60 min to get an amorphous Al_2O_3 layer, then immersed in boiling water for 30 min to form flaky boehmite, and thermally treated again (400 °C, 10 min) to stabilize the inorganic film [21]. Subsequently, the fluoroalkylsilane (FAS) solution commercially known as Dynasylan® SIVO CLEAR EC (Evonik, Essen, Germany) was

dip-coated on the underlying boehmite layer (dipping–withdrawing speed of 2 mm/s and soaking time of 2 min), followed by consolidation at 150 °C for 30 min.

Alumina-based SLIPS samples were instead fabricated using porous Al_2O_3 LF samples with an additional step of infusion with different perfluoropolyether (PFPE) lubricant oils commercially known as Krytox™ GPL 100, 103 and 105 (Chemours, Geneva, Switzerland). These oils were chosen on the basis of their different viscosity increasing from about 12.4 cst for series 100 up to 82 cst for series 103 and 522 cst for series 105 (at 20 °C). Infusion was obtained by immersion (5 min) in the lubricant oils, followed by drying in vertical position for 3–4 h at room temperature to eliminate any lubricant excess. These Al_2O_3-based SLIPS samples were labeled Al_2O_3Kr100, Al_2O_3Kr103 and Al_2O_3Kr105, respectively.

For what concerns silica-based SLIPS samples, the fluorinated silica suspension was deposited via dip coating on aluminum foil with a dipping–withdrawal speed of 2 mm/s and a soaking time of 1 min. After deposition the samples were thermally treated at 150 °C for 30 min allowing the layer to adhere to the substrate. Subsequently, silica-based SLIPS were fabricated by immersion in the different Krytox™ lubricants (GPL 100, 103 and 105) and in silicone oil having a viscosity of 10 cSt (Sigma-Aldrich). Silicone oil was selected as a more environmentally sustainable alternative to fluorinated Krytox™ oils. These SiO_2-based SLIPS samples were labeled SiO_2FKr100, SiO_2FKr103, SiO_2FKr105 and SiO_2FSO10, respectively. The surface tension of the lubricants used for SLIPS fabrication was measured with the pendant drop method performed with an optical system (Drop Shape Analyzer DSA30, Krüss GmbH, Hamburg, Germany).

2.4. Surface Characterization

All surfaces were characterized in terms of repellency against water. The static water contact angle (WCA) was measured with sessile water drops (volume 10 μL) using the Drop Shape Analyzer DSA30. The dynamic wetting, expressed by the contact angle hysteresis (CAH), was evaluated with the needle-in technique [31]. CAH was calculated as the difference between the advancing and the receding contact angle of a sessile drop with a volume of 20 μL. Contact angle values were calculated as the average of five to ten measurements on different points of the surface.

The different morphology of surfaces after deposition of Al_2O_3 or SiO_2 as inorganic layer was investigated with a field emission scanning electron microscope (FESEM Gemini Columns SIGMA, Carl Zeiss Microscopy GmbH, Oberkochen, Germany). Surface characterization has been carried out at subzero temperatures. The WCA and the CAH of coatings were evaluated at temperatures of −2.5, −5, −7.5 and −10 °C via goniometric analysis. To reach the analysis temperature, the samples were placed in an environmental chamber equipped with a Peltier plate (Temperature Control Chamber TC40, Krüss GmbH, Hamburg, Germany). The Peltier system is liquid-cooled with a thermo-cryostat AC150 immersion circulator (ThermoFisher Scientific, Waltham, MA, USA) able to control the temperature in a range from −20 to 80 °C. Surface temperature was monitored with a built-in Pt100 thermocouple. The temperature of water droplets was set at 5 °C.

2.5. Assessment of Durability

Since the liquid repellent surfaces described in this paper are expected to be applied at subzero temperature, they were subjected to freeze/and frost/thaw cycles performed, respectively, in presence or absence of liquid water in contact with the samples. For each condition, the total number of cycles was equal to 10 and they were established in order to evaluate the resistance with respect to the final use environment. Three samples per type were tested to guarantee reproducibility.

In the freeze/thaw cycles, a plastic cylinder was placed on the surfaces and water was poured inside with a liquid column of about 1 cm. Then the samples were transferred into a lab freezer at a temperature of $-10\ ^{\circ}C \pm 1\ ^{\circ}C$ and kept there for 3 h. After, the samples were taken out, ice was allowed to melt and the surfaces were subjected to WCA and CAH measurements. The experimental set up is represented in Figure 3.

Figure 3. Experimental set up for freeze/thaw test. Water contained in the plastic cylinder was allowed to ice in contact with the surfaces.

In the case of frost/thaw cycles, sample surfaces were simply kept in a lab freezer at T of −10 °C ± 1 °C for 3 h, allowing frost formation Then, the samples were taken out, ice was allowed to melt and the samples were subjected to WCA and CAH measurements.

3. Results and Discussion

3.1. Wetting Behavior at Room Temperature and Surface Morphology

The wetting data of the different coating typologies are shown in Table 2 together with those referring to an uncoated aluminum surface taken as reference. Alumina-based coatings with FAS as the organic layer (LF series) present outstanding liquid repellency reaching static and dynamic superhydrophobicity with WCA of about 170° and CAH < 10°. Meanwhile, SLIPS samples showed WCA values as high as 120° and CAH in any case equal to or lower than 10°.

Table 2. Average static contact angle with water (WCA) and contact angle hysteresis (CAH) at T_{amb}.

Sample	WCA (°) ± ⌈ (°)	CAH (°) ± ⌈ (°)
Uncoated sample (Ref.)	89 ± 2	59 ± 7
LF	171 ± 2	7 ± 2
Al_2O_3 Kr100	121 ± 1	2 ± 1
Al_2O_3 Kr103	122 ± 1	3 ± 1
Al_2O_3 Kr105	119 ± 2	9 ± 1
SiO_2F SO10	112 ± 2	10 ± 2
SiO_2F Kr100	123 ± 4	6 ± 2
SiO_2F Kr103	123 ± 4	6 ± 2
SiO_2F Kr105	119 ± 5	9 ± 1

More in detail, while the different viscosities of Krytox™ oils seem not to affect the static performance (WCA) of coated surfaces, their dynamic behavior is optimized (CAH as low as 2–3°) when low viscosity lubricants (Kr100 and Kr103) are infused. On these surfaces, drag forces against the sliding of the water drops are particularly reduced so that the sticking of the liquid can be almost completely avoided.

Silica-based SLIPS infused with Krytox™ GPL oils exhibited quite the same wetting behavior compared with the Al_2O_3-based SLIPS samples. Using silicone oil as the lubricant leads to a small decrease of the WCA to 112° and a slight increase of the CAH to 10°, respectively. The decrease of WCA might be explained considering the surface tension, γ, of the different oils. Silicone oil has a slightly higher γ than Krytox™ oils (see Table 3). As known in literature, the higher the gap in surface tension between the lubricant and water (γ = 72 mN/m at T = 20 °C), the higher the WCA.

As shown in the table, silicone oil has a higher surface tension than Krytox™ oils which means a lower gap in γ between water and the lubricant. This leads to a decrease of anti-wetting performance for SiO_2-based SLIPS infused in silicone oil, while maintaining an acceptable degree of both static and dynamic repellence.

Table 3. Surface tensions (γ) and viscosity (μ) of the four lubricants used for the fabrication of and slippery liquid infused porous surfaces (SLIPS).

Lubricant Oil	γ (mN/m) ± ∫ (mN/m)	μ (cSt)
Krytox™100	16.60 ± 0.04	12.4 [1]
Krytox™103	17.41 ± 0.01	82 [1]
Krytox™105	18.35 ± 0.08	522 [1]
Silicone Oil 10cst	20.01 ± 0.30	9–11 [2]

[1] Chemours Technical Specifications of Krytox™ GPL series oils; [2] Sigma-Aldrich Product Specification Sheet.

Figures 4 and 5 show the morphology obtained after deposition of alumina and fluorine-rich silica layers, respectively. Alumina nanoparticles, after the structuring process in boiling water, leads to the formation of the typical hierarchically organized "flower-like" structure. The surface structure presents voids with dimensions of about 50 nm [30], able to host and trap either air pockets (LF surfaces) or lubricants (SLIPS).

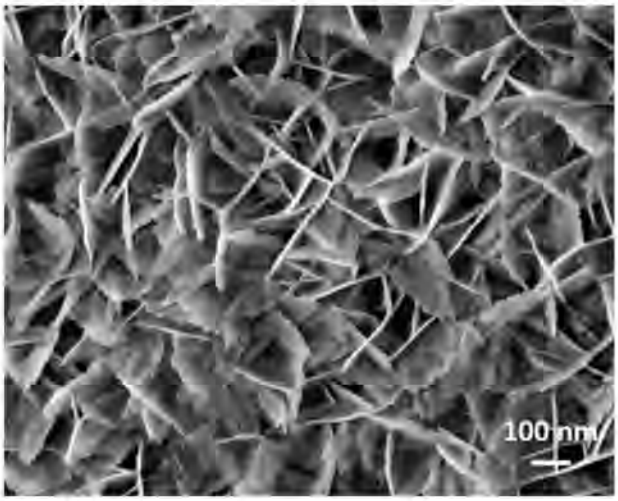

Figure 4. Micrograph of nanostructured Al_2O_3 inorganic layer.

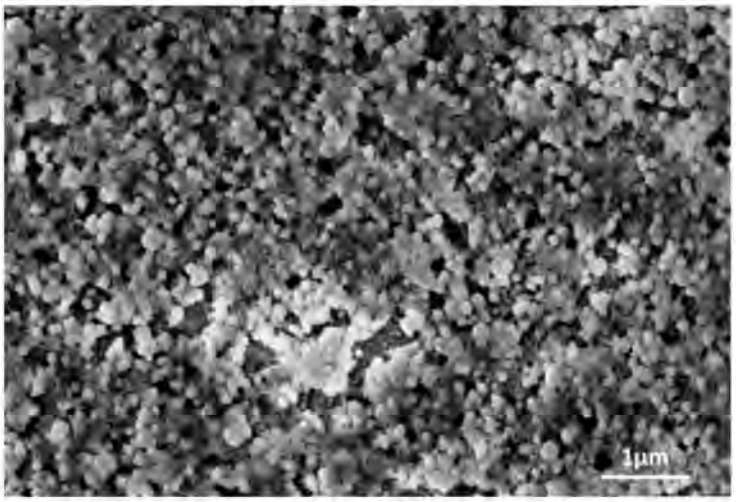

Figure 5. Micrograph of nanostructured SiO_2 inorganic layer.

The following functionalization with FAS molecules did not alter the coating morphology. FAS molecules form a monolayer on boehmite surfaces, as demonstrated in a previous work [32].

The deposition of fluorinated silica involves the formation of nanoparticle agglomerates well distributed on the whole surface area, as shown in Figure 5.

3.2. Wetting Behavior at Low Temperatures

At subzero temperatures, coated surfaces suffered from a general worsening of both WCA and CAH values compared to those detected at room temperature. Moreover, the repellency against water is influenced by a different amount depending on the design approaches and coatings composition.

The average values of WCA detected on the different coated samples in the temperature range between −2.5 and −10 °C are collected in the histogram of Figure 6 (WCA @T < 0 °C, green bars). WCA of each surface coating was stable over this range of temperatures. The spreading and retraction dynamics of the droplets at subzero temperatures are instead reported in Figure 7 showing the CAH values (see Section 2.4). The retraction dynamic of drops is particularly interesting. The change in the receding contact angle resulting from ice nucleation de facto reduces the surface tension-based retraction force that acts radially inwardly. It is such a force that mimics the desired de-wetting behavior [33].

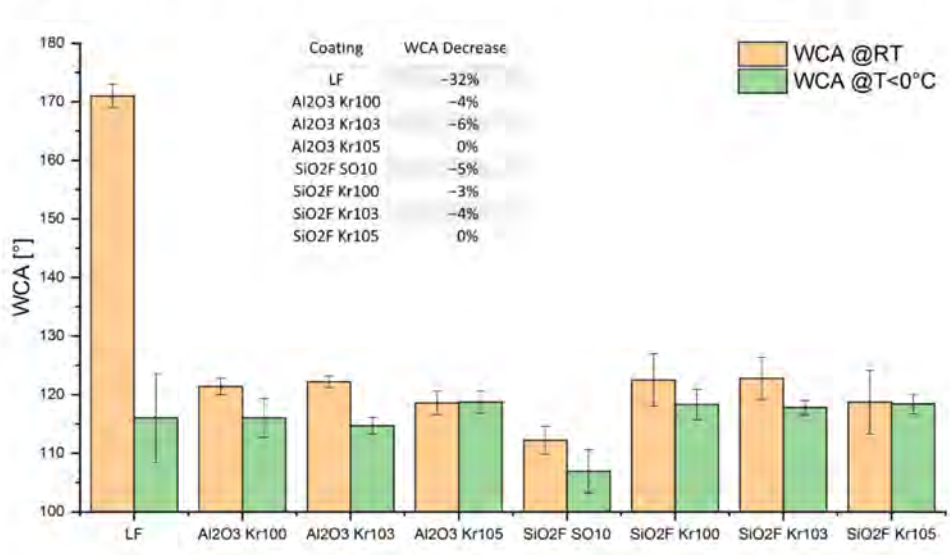

Figure 6. Static water contact angle (WCA) measurements at ambient temperature (WCA @RT in the graph legend) and the average values of WCA detected on the different coated samples in the temperature range between −2.5 and−10 °C (WCA @T < 0 °C in the graph legend). The table produced as inset reports the percentage decrease of WCA between RT and T < 0 °C.

In particular, when the temperature is decreasing, LF surfaces suffer from a greater reduction of liquid repellency with respect to the SLIPS ones. This can be ascribed to the Cassie-to-Wenzel transition (CWT) [34–39], which leads to the penetration of the water drops inside the nanostructure, eliminating the air pockets needed to suspend the liquids with the consequent appearance of adhesion phenomena between the liquid and the surface. The occurrence of irreversible CWT for superhydrophobic surfaces exposed to icing conditions has been already reported [40–42] due to capillary condensation of water vapor between surface features [43]. This phenomenon has been confirmed by non-restored initial values of WCA and CAH when the samples returned at room temperature, which confirms the irreversible CWT just after a single exposure at temperature lower than 0 °C. Compared to the performance at room temperature, the WCA of LF samples decreased from 171° to about 116° and the CAH increased from 7° to 35°, which led to a loss of mobility of the drops. The poor stability of the LF coatings at low temperature makes them unsuitable for applications in cold environments. As far as the SLIPS approach, the wetting behavior detected at subzero temperature resulted quite unchanged with respect to that observed at room temperature, particularly when CAH is concerned.

Compared with LF samples all SLIPS exhibited much lower CAH at each subzero temperature, maintaining the values below 15°. This means that a proper dynamic anti-wetting ability was also kept in a supercooling environment.

The minimum decrease of CAH compared to LF samples has been measured on Al_2O_3 as the inorganic layer and Krytox™ 105 oil as the infused lubricant; furthermore, Krytox™ 105 gives the worst performance on both underlying silica and alumina layers due to its large viscosity (see Table 3) that hinders drop mobility [44]. Despite the satisfactory results in terms of wetting behavior at each tested temperature with both alumina and fluorinated silica as the inorganic layer, Krytox™ 100 presented issues regarding the depletion of the oil during the course of the experiment.

This was probably due to the evaporation of Krytox™ 100 that even at room temperature has more tendency to leave uncovered the underlying structure. Hence, after the tests the samples lubricated with Krytox™ 100 lost their liquid repellency. SLIPS infused with Krytox™ GPL 103 and 105 did not exhibit this issue, due to the low evaporation rate of these oils [13]. The same wetting behavior is observed with both inorganic phases infused with lubricant oils, with no particular differences between samples coated with SiO_2 or Al_2O_3. Surfaces infused with silicone oil exhibited the same durability of samples infused with fluorinated lubricants, while keeping WCA and CAH unchanged. All the coatings reported in Figure 7 have been selected as candidate coatings to undergo the durability test of Section 3.3, except for the Al_2O_3Kr100 and SiO_2FKr100 coatings due to the aforementioned oil evaporation issues.

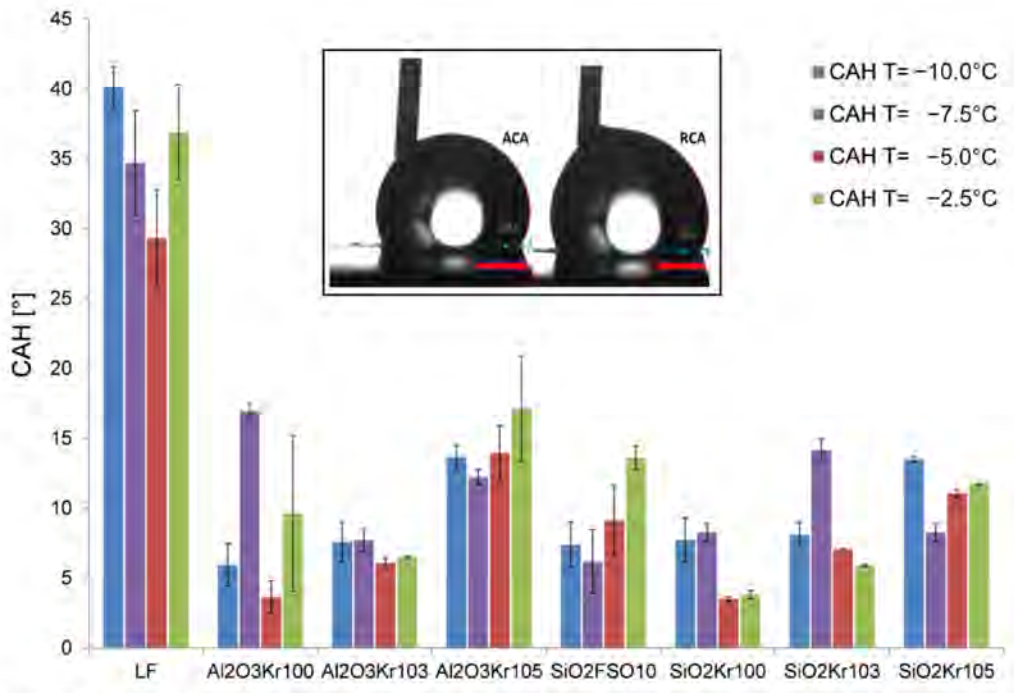

Figure 7. Contact angle hysteresis (CAH) of the surface coatings grouped by coating type. Standard deviations are reported as error bars. Drop profiles used for advancing and receding contact angle (ACA and RCA, respectively) of one of the measurements on Al2O3Kr100-infused sample are reported as inset.

3.3. Durability

The durability of coated surfaces is a key issue in view of practical applications, because it influences the end use of the designed materials or the environment to which they could be exposed. In particular we refer to durability as the ability to withstand degradation or wearing out in use. Very often the loss of performances over the time and/or under harsh conditions represents a very severe limitation for the technology

transfer from the lab to the production scale. In addition, in many cases the understanding of the environmental conditions to be simulated is critical so that the choice of appropriate tests allowing evaluating the integrity of material performances over its lifecycle is not obvious. We chose to analyze two different ice accretion conditions, namely freezing (i.e., solidification of liquid water) and frosting (condensation of humid air), and their effect on the wetting properties of the coatings.

The results of the freeze/thaw tests are here discussed as a function of the different design approaches and coating compositions.

In details, the sampling included the following surfaces:

- LF (used as reference);
- Al_2O_3 Kr103 and Al_2O_3 Kr105;
- SiO_2F Kr103 and SiO_2F Kr105;
- SiO_2F SO10.

CAH on the different sample surfaces was measured after one freeze/thaw cycle and compared with that of untreated samples (Figure 8). The CAH value was calculated as the average of 10 different measurements performed on the surface area in contact with water along the test.

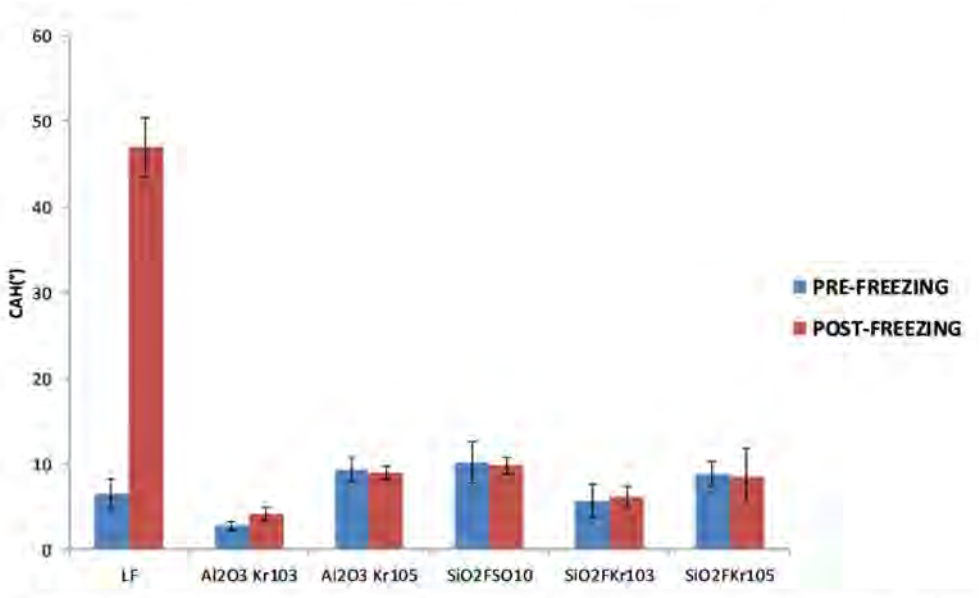

Figure 8. Average values of contact angle hysteresis (CAH) for selected coated samples before (blue) and after a single freeze/thaw cycle (red). Standard deviations are reported as errors bars.

According to CAH results, LF samples lost their dynamic liquid repellency after performing a single freeze/thaw cycle, with a huge increase of CAH. As expected on the basis of the current literature, LF coatings revealed to be heavily affected by ice formation.

SEM images of Figure 9 clearly show a significant flattening of the flower-like structures, which become unable to trap air between its features with the consequent Cassie-to-Wenzel transition leading to a complete absence of drop mobility on the surface due to the increasing of liquid–solid adhesion forces. Specifically, Figure 9b shows a damaged area of the LF sample where only a small portion (light spots) of the nanostructured boehmite is still intact, while darker areas no longer possess the flower-like nanostructure.

On the contrary, Al_2O_3 and SiO_2-based SLIPS preserved both static and dynamic anti-wetting performances after the first freeze/thaw cycle. SLIPS samples underwent 10 freeze/thaw cycles to evaluate the resistance of the surfaces. The values of CAH after each cycle are shown in Figure 10; furthermore, some SEM micrographs of SiO_2-based SLIP surfaces registered at the end of the cycles are provided in the Supporting Information. Even if the interest for the surfaces is in a clear depletion of the lubricant with respect to the

initial state, the nanostructures remain partly infused (refer to Figure S1 of the Supporting Information).

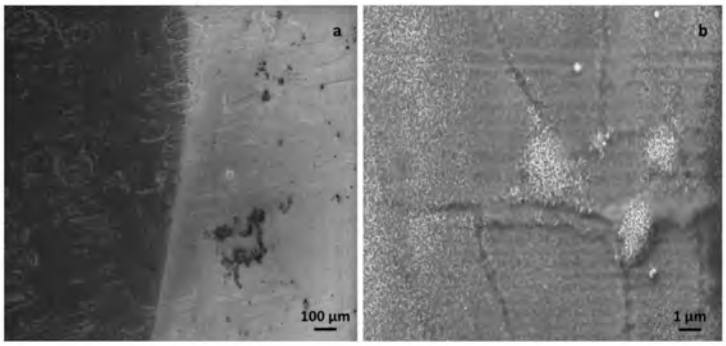

Figure 9. (**a**) Micrographs of LF surfaces after freeze/thaw test; the dark zone was in contact with water during icing while the clear one was water-free during the test. (**b**) High magnification of the frozen zone which exhibits the flattening of the flower-like structure after the test.

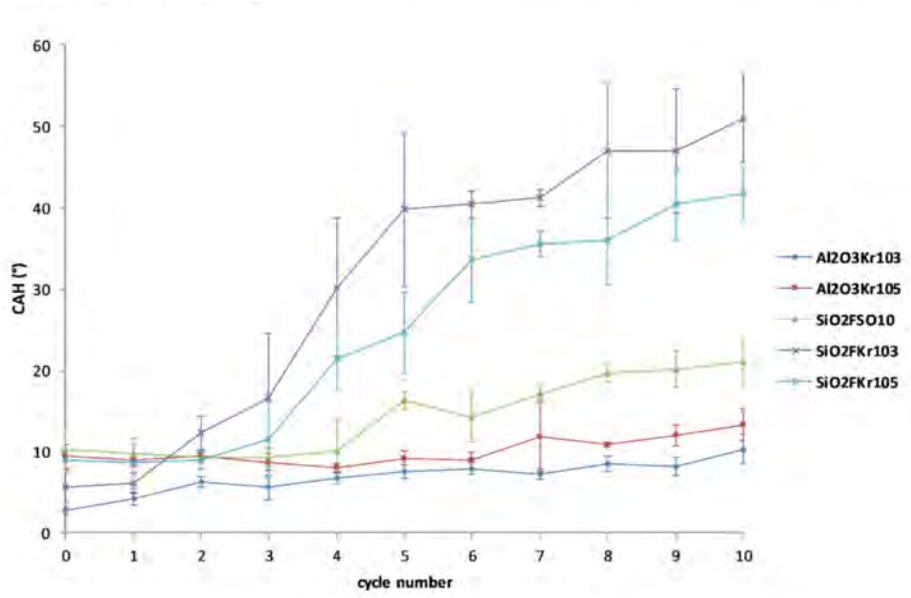

Figure 10. Contact angle hysteresis (CAH) as a function of the freeze/thawing cycle number. Standard deviations are reported as error bars.

Alumina-based SLIPS maintained their performance after 10 freeze/thaw cycles, with a slight increase of CAH which, however, never exceeded 15°. This means that after the test the drop mobility on Al_2O_3 SLIPS surfaces was preserved.

Comparing the performance of Al_2O_3 and SiO_2F SLIPS samples, it was noticed an effect of nanostructure on durability. Using SiO_2 as the inorganic layer and Krytox™ as the lubricant, the samples exhibit a remarkable increase of CAH after 3 freeze/thaw cycles, passing from about 10° to 20/30°. After the last cycle the CAH of SiO_2F SLIPS overcame 40°, with complete absence of drops mobility on the surface. The different behavior could be due to the large pores in SiO_2 nanostructure (see Figure 5) which might cause a low capillary pressure and therefore a low retention of the oil between the surface features. The formation of these holes is probably due to the formation of agglomerates of nanoparticles, unable to homogeneously cover the whole surface. The dimensions of the holes observed by SEM analysis might be confirming evidence of this hypothesis. The Al_2O_3 "flower-like" nanostructure presents interstitial cavities with size close to 50 nm (see Figure 4), while the deposition of SiO_2F suspension leads to the formation of holes which reach sizes of even 1 µm (see Figure 5). In the latter case, the cavities might not be narrow enough to

guarantee the right anchorage of the lubricants and at the same time they allow water to penetrate within the surface structure. At the scale of the surface nanostructures, the main responsibility for the immobilization of the lubricant is the capillary force (refer to Figures 4 and 5 for alumina and silica nanostructures, respectively). In particular over the top of the nanostructures, it is precisely the capillary force that determines the nanoscale wettability, e.g., whether or not a continuous layer of lubricant is formed over the surface topography. The equilibrium film thickness is in fact the result of the balancing of the cohesive surface tension that draws the lubricant away and intermolecular forces that stabilize it. Through the cycles of the durability tests, the lubricant can be increasingly removed from the top of the nanostructures. If not "healed", the lubricant depletion will lead to the loss of hydrophobic behavior. Just in case of lubricant depletion from the top of the nanostructures, the lubricant that remains within the nanostructures might more or less easily restore the pristine situation if it has more or less tendency to spread "uphill". The more is this tendency, the more self-healing the SLIPS will be.

Using a simple macroscopic model (the Dzyaloshinskii-Lifshitz-Pitaevskii or DLP model) we can calculate a rough estimate of the van der Waals interaction portion of the interface potential for Krytox™-infused SLIPS with both fluorinated silica and alumina. The sign of the Hamaker constant indicates the nature of the interaction between flat layers. If the Hamaker constant is negative then the VdW force is positive (repulsive), and the system results with a stable sandwiched layer of infused oil. Though the considered system is on the edge of the DLP's limit (please refer to the Supporting Information), the obtained repulsive forces for alumina SLIPS result in being an order of magnitude larger than those one for the silica (see Figure S2 of the Supporting Information). The more repulsive the VdW forces are, the more wetting tendency of the infused oil there will be, and the underneath surface might easily recover the pristine oil-infused state. Even if rough, this model seems to catch that the silica SLIPSs show a less pronounced capillary action than the alumina SLIPSs., and the observed loss of performance of the silica SLIPSs after only a few freeze/thaw cycles might in part be due to such a phenomenon.

Samples coated with SiO_2F nanoparticles and infused with silicone oil (SiO_2FSO10) exhibited an increase of CAH after the 4th freezing cycle, passing from 10° to about 16°. After the 4th cycle, the CAH remained quite constant in a range of around 16–20°, which means an acceptable mobility of the drops on the surfaces. The chemical affinity between silica and silicone oil provides a better adsorption compared to the Krytox™ fluoro-based lubricant. We presume that this effect promotes the silicone oil retention on the surface. The silicone layer is a barrier that prevents the water from getting in contact with the nanostructure below, in a way to preserve the hydrophobic property along the freezing cycles. The effect of nanostructure on resistance at low temperature will be the object of future studies in order to understand the role of the coating composition on stability at temperatures lower than 0 °C.

The same samples used for the freeze/thaw test underwent a frost/thaw test, also carried out in the freezer at -10 °C $\pm$ 1 °C but with no water put in contact with the surfaces. The frost/thaw durability test results are shown in Figure 11.

As for the freeze/thaw test, LF samples presented a big increase of adhesion forces between water and surfaces just after a single frost/thaw cycle, with CAH passing from 6 to 66 °C (not reported for brevity). This is due to the replacement of the bubble of air trapped in the nanostructure led by the condensation of environment water at temperature below 0 °C. The same phenomenon has been observed during the CAH measurements at T < 0 °C, in which the LF samples irreversibly lost their performance just after a single exposure in a freezing environment. Concerning SLIPS samples, all the surfaces maintained the CAH quite unchanged after 10 frost/thaw cycles, with CAH values between 5 and 10 °C. In this case the lubricant layer acts like an insulator which avoids the contact of the environmental water vapor with the nanostructure and its consequent condensation. Comparing the frosting results with the freezing ones, a remarkable effect of the freezing water in contact with the surfaces is noticed, especially when using SiO_2 as inorganic layer. The values

of CAH for SiO_2 infused in fluorinated lubricant were retained throughout the entire frost/thaw tests, while during freeze/thaw tests the performance was lost after few cycles. This different behavior, coupled with the presumed capillary effect discussed before, may be explained considering the penetration of water in the pores of the coatings. When putting liquid water in contact with the surface as in freeze/thaw tests, the lubricant layer has to support a much higher pressure with respect to the force applied with no contact water. Probably the pressure present during freezing was too high with the consequent lubricant film collapse, allowing the transport of lubricant out of the freezing zone (refer to Figure 3 and Figure S1 of the Supporting Information). In addition, the penetration of the water inside the pores led to a further loss of anti-wetting performance because of the drainage of lubricant reservoir. Due to the size of the pores, the flower-like structure offered by the Al_2O_3 inorganic coating results in being more suitable to support the pressure applied by the liquid water coupled with less drainage of lubricant oils from it and a consequent effective self-healing capacity. The design of Al_2O_3 SLIPS led to a complete stability of CAH values over both freezing and frosting cycles.

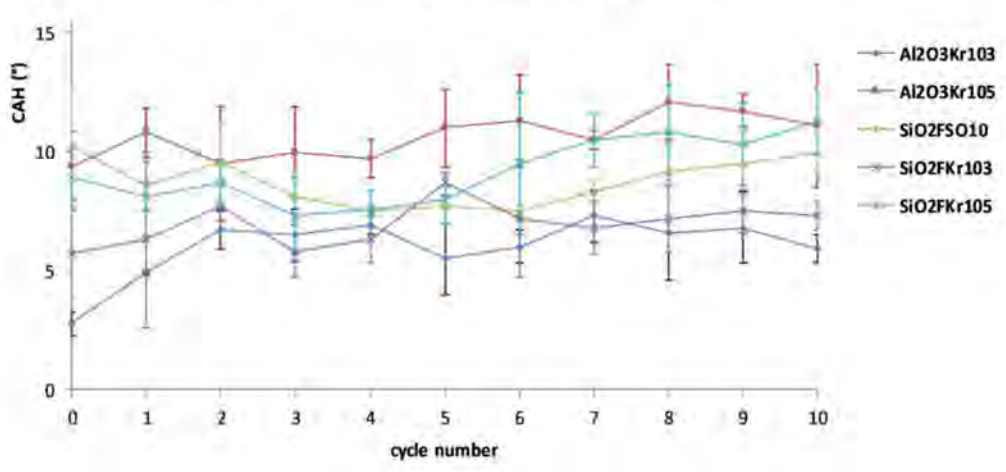

Figure 11. CAH vs. frost/thaw cycle number. Standard deviations are reported as error bars.

4. Conclusions

The present study was aimed at the design and development of biomimetic coatings with a potential for the mitigation of icing issues. The process started with the synthesis of different suspensions of ceramic oxide nanoparticles via sol-gel route. We first designed a hybrid inorganic-organic coating based on nanostructured alumina and a grafted fluorinated organic polymer, and a facile, green and low-cost coating based on fluorinated SiO_2 nanoparticles deposited by a single step process. We also explored a different approach to liquid repellency, as per the so-called SLIPS approach. We added low surface tension lubricants—different types of fluorinated Krytox™ GPL and a silicone oil—with different viscosities and chemical compositions to explore their different behaviors when infused in the hybrid-coated surfaces.

We studied the static and dynamic wetting behavior on the fabricated low-wettable coatings at room and subzero temperatures. In particular we report evidence of stable static water contact angle and low water contact angle hysteresis of all the SLIPS coatings in the temperature range from −10 to 0 °C. Quite remarkably, high drop mobility also was achieved at temperatures below 0 °C. Comparing the performance of fabricated samples, it was noticed that SLIPS infused in Krytox™ GPL 103 oil provided the best wetting properties at subzero temperature.

The durability of fabricated low-wettable surfaces was also investigated by monitoring the evolution of their wetting properties after ice accretion in two different conditions (i.e., freezing and frosting). All the investigated surfaces showed a good resistance along frosting test, with the only exception of LF samples. After 10 frost/thaw cycles, the CAH

values resulted unchanged using both SiO_2 and Al_2O_3 nanoparticles as inorganic layers. Concerning the freezing test, only Al_2O_3 SLIPS kept the CAH values stable along cycles while SiO_2F SLIPS covered with Krytox™ oils lost their performance after few exposures in the icing environment. SiO_2 SLIPS infused in silicone oil suffered a slight increase of CAH after the third cycle but then the values remained stable until the last exposure. These results highlight the potential of SLIPS in those application fields in which dynamic water repellency at subzero temperature is crucial (e.g., aeronautics, telecommunications, etc.). Moreover, it is important to carefully consider the icing environments that low-wettable surfaces will face once in operation. SLIPS design and engineering must account for possible oil depletion phenomena in order to achieve durable water repellency when exposed at subzero temperature. In perspective of future large-scale application of the presented solutions, it must be said that SLIPS formulations have a higher cost than LF ones due to the addition of the lubricant; moreover, fluorinated lubricants like Krytox have a significantly higher price than fluorine-free liquids like silicone oil. However, their excellent repellence and enhanced durability at subzero temperatures can justify such cost difference, especially for high-added value applications, i.e., aircraft surfaces.

Supplementary Materials: The following are available online at https://www.mdpi.com/2079-6412/11/1/77/s1. Figure S1. (a) SEM micrograph of the freezing zone of SiO_2SO10 surface after freeze/thaw test; (b) SEM micrograph of the freezing zone of SiO_2Kr105 surface after freeze/thaw test; (c) and (d) are instead reported as example of lubricant accumulation on the border zones for SiO_2SO10 and SiO_2Kr105 respectively, Figure S2. Dispersion energy term vs Krytox™ lubricant thickness with both Silica and Alumina layers.

Author Contributions: The manuscript was written through contributions of all authors. G.B. and A.C. contributed equally sharing the authorship. Conceptualization, M.R. with the support of G.B., A.C.; methodology, G.B., A.C.; validation, G.B., A.C.; formal analysis, G.B., A.C.; investigation, G.B., A.C., with the support of F.V.; resources, ISTEC-CNR; data curation, G.B., A.C.; writing—original draft preparation, G.B., A.C.; writing—review and editing, G.B., A.C., F.V., M.R.; visualization, G.B., A.C.; supervision, M.R.; project administration, G.B., A.C.; M.R.; funding acquisition, M.R. All authors have read and agreed to the published version of the manuscript.

Funding: This research received no external funding.

Institutional Review Board Statement: Not applicable.

Informed Consent Statement: Not applicable.

Data Availability Statement: Data is contained within the article or supplementary material.

Conflicts of Interest: The authors declare no conflict of interest.

References

1. Laforte, J.L.; Allaire, M.A.; Laflamme, J. State-of-the-art on power line de-icing. *Atmos. Res.* **1998**, *46*, 143–158. [CrossRef]
2. Farzaneh, M.; Volat, C.; Leblond, A. Anti-icing and de-icing techniques for overhead lines. In *Atmospheric Icing of Power Networks*; Springer: Dordrecht, The Netherlands, 2008; pp. 229–268. [CrossRef]
3. Egbert, R.I.; Schrag, R.L.; Bernhart, W.D.; Zumwalt, G.W.; Kendrew, T.J. An investigation of power une de-icing by electro-impulse methods. *IEEE Trans. Power Deliv.* **1989**, *4*, 1855–1861. [CrossRef]
4. Poots, G.; Gent, R.W.; Dart, N.P.; Cansdale, J.T. Aircraft icing. *Philos. Trans. R. Soc. London. Ser. A Math. Phys. Eng. Sci.* **2000**, *358*, 2873–2911.
5. Susoff, M.; Siegmann, K.; Pfaffenroth, C.; Hirayama, M. Evaluation of icephobic coatings—Screening of different coatings and influence of roughness. *Appl. Surf. Sci.* **2013**, *282*, 870–879. [CrossRef]
6. Guo, P.; Zheng, Y.; Wen, M.; Song, C.; Lin, Y.; Jiang, L. Icephobic/Anti-Icing Properties of Micro/Nanostructured Surfaces. *Adv. Mater.* **2012**, *24*, 2642–2648. [CrossRef]
7. Kraj, A.G.; Bibeau, E.L. Phases of icing on wind turbine blades characterized by ice accumulation. *Renew. Energy* **2010**, *35*, 966–972. [CrossRef]
8. Meuler, A.J.; Smith, J.D.; Varanasi, K.K.; Mabry, J.M.; McKinley, G.H.; Cohen, R.E. Relationships between water wettability and ice adhesion. *ACS Appl. Mater. Interfaces* **2010**, *2*, 3100–3110. [CrossRef] [PubMed]
9. Narhe, R.D.; Beysens, D.A. Growth dynamics of water drops on a square-pattern rough hydrophobic surface. *Langmuir* **2007**, *23*, 6486–6489. [CrossRef] [PubMed]

10. Varanasi, K.K.; Deng, T.; Smith, J.D.; Hsu, M.; Bhate, N. Frost formation and ice adhesion on superhydrophobic surfaces. *Appl. Phys. Lett.* **2010**, *97*, 234102. [CrossRef]
11. Cao, L.; Jones, A.K.; Sikka, V.K.; Wu, J.; Gao, D. Anti-Icing Superhydrophobic Coatings. *Langmuir* **2009**, *25*, 12444–12448. [CrossRef] [PubMed]
12. He, M.; Wang, J.; Li, H.; Song, Y. Super-hydrophobic surfaces to condensed micro-droplets at temperatures below the freezing point retard ice/frost formation. *Soft Matter* **2011**, *7*, 3993–4000. [CrossRef]
13. Zhang, Q.; Jin, B.; Wang, B.; Fu, Y.; Zhan, X.; Chen, F. Fabrication of a highly stable superhydrophobic surface with dual-scale structure and its antifrosting properties. *Ind. Eng. Chem. Res.* **2017**, *56*, 2754–2763. [CrossRef]
14. Lynch, F.T.; Khodadoust, A. Effects of ice accretions on aircraft aerodynamics. *Prog. Aerosp. Sci.* **2001**, *37*, 669–767. [CrossRef]
15. Song, J.; Zhao, D.; Han, Z.; Xu, W.; Lu, Y.; Liu, X.; Liu, B.; Carmalt, C.J.; Deng, X.; Parkin, I.P. Super-robust superhydrophobic concrete. *J. Mater. Chem. A* **2017**, *5*, 14542–14550. [CrossRef]
16. Zhan, X.; Yan, Y.; Zhang, Q.; Chen, F. A novel superhydrophobic hybrid nanocomposite material prepared by surface-initiated AGET ATRP and its anti-icing properties. *J. Mater. Chem. A* **2014**, *2*, 9390–9399. [CrossRef]
17. Jung, S.; Dorrestijn, M.; Raps, D.; Das, A.; Megaridis, C.M.; Poulikakos, D. Are superhydrophobic surfaces best for icephobicity? *Langmuir* **2011**, *27*, 3059–3066. [CrossRef]
18. Verho, T.; Bower, C.; Andrew, P.; Franssila, S.; Ikkala, O.; Ras, R.H. Mechanically durable superhydrophobic surfaces. *Adv. Mater.* **2011**, *23*, 673–678. [CrossRef]
19. Cheng, Y.T.; Rodak, D.E. Is the lotus leaf superhydrophobic? *Appl. Phys. Lett.* **2005**, *86*, 1–3. [CrossRef]
20. Wong, T.S.; Kang, S.H.; Tang, S.K.; Smythe, E.J.; Hatton, B.D.; Grinthal, A.; Aizenberg, J. Bioinspired self-repairing slippery surfaces with pressure-stable omniphobicity. *Nature* **2011**, *477*, 443–447. [CrossRef]
21. Niemelä-Anttonen, H.; Koivuluoto, H.; Tuominen, M.; Teisala, H.; Juuti, P.; Haapanen, J.; Harra, J.; Stenroos, C.; Lahti, J.; Kuusipalo, J.; et al. Icephobicity of slippery liquid infused porous surfaces under multiple freeze—thaw and ice accretion—detachment cycles. *Adv. Mater. Interfaces* **2018**, *5*, 1800828.
22. Kim, P.; Wong, T.S.; Alvarenga, J.; Kreder, M.J.; Adorno-Martinez, W.E.; Aizenberg, J. Liquid-infused nanostructured surfaces with extreme anti-ice and anti-frost performance. *ACS Nano* **2012**, *6*, 6569–6577. [CrossRef] [PubMed]
23. Wei, C.; Jin, B.; Zhang, Q.; Zhan, X.; Chen, F. Anti-icing performance of super-wetting surfaces from icing-resistance to ice-phobic aspects: Robust hydrophobic or slippery surfaces. *J. Alloys Compd.* **2018**, *765*, 721–730. [CrossRef]
24. Wexler, J.S.; Jacobi, I.; Stone, H.A. Shear-driven failure of liquid-infused surfaces. *Phys. Rev. Lett.* **2015**, *114*, 168301. [CrossRef] [PubMed]
25. Lee, H.; Alcaraz, M.L.; Rubner, M.F.; Cohen, R.E. Zwitter-wettability and antifogging coatings with frost-resisting capabilities. *ACS Nano* **2013**, *7*, 2172–2185. [CrossRef]
26. Mishchenko, L.; Hatton, B.; Bahadur, V.; Taylor, J.A.; Krupenkin, T.; Aizenberg, J. Design of ice-free nanostructured surfaces based on repulsion of impacting water droplets. *ACS Nano* **2010**, *4*, 7699–7707. [CrossRef]
27. Khedir, K.R.; Kannarpady, G.K.; Ishihara, H.; Woo, J.; Asar, M.P.; Ryerson, C.; Biris, A.S. Temperature-dependent bouncing of super-cooled water on teflon-coated superhydrophobic tungsten nanorods. *Appl. Surf. Sci.* **2013**, *279*, 76–84. [CrossRef]
28. Schutzius, T.M.; Jung, S.; Maitra, T.; Eberle, P.; Antonini, C.; Stamatopoulos, C.; Poulikakos, D. Physics of icing and rational design of surfaces with extraordinary icephobicity. *Langmuir* **2015**, *31*, 4807–4821. [CrossRef]
29. Sarshar, M.A.; Swarctz, C.; Hunter, S.; Simpson, J.; Choi, C.-H. Effects of contact angle hysteresis on ice adhesion and growth on superhydrophobic surfaces under dynamic flow conditions. *Colloid Polym. Sci.* **2013**, *291*, 427–435. [CrossRef]
30. Raimondo, M.; Blosi, M.; Caldarelli, A.; Guarini, G.; Veronesi, F. Wetting behavior and remarkable durability of amphiphobic aluminum alloys surfaces in a wide range of environmental conditions. *Chem. Eng. J.* **2014**, *258*, 101–109. [CrossRef]
31. Kleingartner, J.A.; Srinivasan, S.; Mabry, J.M.; Cohen, R.E.; McKinley, G.H. Utilizing dynamic tensiometry to quantify contact angle hysteresis and wetting state transitions on nonwetting surfaces. *Langmuir* **2013**, *29*, 13396–13406. [CrossRef]
32. Motta, A.; Cannelli, O.; Boccia, A.; Zanoni, R.; Raimondo, M.; Caldarelli, A.; Veronesi, F. A mechanistic explanation of the peculiar amphiphobic properties of hybrid organic-inorganic coatings by combining XPS characterization and DFT modeling. *ACS Appl. Mater. Interfaces* **2015**, *7*, 19941–19947. [CrossRef] [PubMed]
33. Bahadur, V.; Mishchenko, L.; Hatton, B.; Taylor, J.A.; Aizenberg, J.; Krupenkin, T. Predictive model for ice formation on superhydrophobic surfaces. *Langmuir* **2011**, *27*, 14143–14150. [CrossRef] [PubMed]
34. Tsai, P.; Lammertink RG, H.; Wessling, M.; Lohse, D. Evaporation-triggered wetting transition for water droplets upon hydrophobic microstructures. *Phys. Rev. Lett.* **2010**, *104*, 2–3. [CrossRef] [PubMed]
35. McCarthy, M.; Gerasopoulos, K.; Enright, R.; Culver, J.N.; Ghodssi, R.; Wang, E.N. Biotemplated hierarchical surfaces and the role of dual length scales on the repellency of impacting droplets. *Appl. Phys. Lett.* **2012**, *100*, 1–6. [CrossRef]
36. Papadopoulos, P.; Mammen, L.; Deng, X.; Vollmer, D.; Butt, H.J. How superhydrophobicity breaks down. *Proc. Natl. Acad. Sci. USA* **2013**, *110*, 3254–3258. [CrossRef]
37. Bormashenko, E.; Pogreb, R.; Whyman, G.; Erlich, M. Cassie-Wenzel wetting transition in vibrating drops deposited on rough surfaces: Is the dynamic Cassie-Wenzel wetting transition a 2D or 1D affair? *Langmuir* **2007**, *23*, 6501–6503. [CrossRef]
38. Lafuma, A.; Quéré, D. Superhydrophobic states. *Nat. Mater.* **2003**, *2*, 457–460. [CrossRef]
39. Bartolo, D.; Bouamrirene, F.; Verneuil, E.; Buguin, A.; Silberzan, P.; Moulinet, S. Bouncing or sticky droplets: Impalement transitions on superhydrophobic micropatterned surfaces. *Europhys. Lett.* **2006**, *74*, 299–305. [CrossRef]

40. Wilson, P.W.; Lu, W.; Xu, H.; Kim, P.; Kreder, M.J.; Alvarenga, J.; Aizenberg, J. Inhibition of ice nucleation by slippery liquid-infused porous surfaces (SLIPS). *Phys. Chem. Chem. Phys.* **2013**, *15*, 581–585. [CrossRef]
41. Kulinich, S.A.; Farhadi, S.; Nose, K.; Du, X.W. Superhydrophobic surfaces: Are they really ice-repellent? *Langmuir* **2011**, *27*, 25–29. [CrossRef]
42. Karmouch, R.; Ross, G.G. Experimental study on the evolution of contact angles with temperature near the freezing point. *J. Phys. Chem. C* **2010**, *114*, 4063–4066. [CrossRef]
43. Stamatopoulos, C.; Hemrle, J.; Wang, D.; Poulikakos, D. Exceptional anti-icing performance of self-impregnating slippery surfaces. *ACS Appl. Mater. Interf.* **2017**, *9*, 10233–10242. [CrossRef] [PubMed]
44. Smith, J.D.; Dhiman, R.; Anand, S.; Reza-Garduno, E.; Cohen, R.E.; McKinley, G.H.; Varanasi, K.K. Droplet mobility on lubricant-impregnated surfaces. *Soft Matter* **2013**, *9*, 1772–1780. [CrossRef]